Magnetic and electronic properties of binary alloy monolayers: Fe_xMn_{1-x} and $Co_{1-x}Fe_x$ on W(110)

M. Pratzer and H. J. Elmers
Institut für Physik, Johannes Gutenberg-Universität Mainz, Staudingerweg 7, D-55099 Mainz, Germany
(Received 16 October 2003; revised manuscript received 19 December 2003; published 15 April 2004)

Pseudomorphic binary alloy monolayers Fe_xMn_{1-x} and $Co_{1-x}Fe_x$ were grown on W(110) by molecular-beam epitaxy in ultrahigh vacuum. Fe atoms are randomly replaced by Mn or Co atoms. The pseudomorphic monolayers form extended areas of monolayer coverages at elevated temperatures in the step flow growth mode. For Fe_xMn_{1-x}/W(110) monolayers the Kerr rotation decreases with decreasing Fe concentration, corresponding to a decrease of the magnetization of $\Delta\mu/\Delta x = -(8\pm2)\mu_B$/atom. The Curie temperature decreases with a rate of $[\Delta T_C(x)/\Delta x]/T_C(\mathrm{Fe}) = -(1.8\pm0.2)\times10^{-2}$ /at. %. Scanning tunneling spectroscopy reveals characteristic maxima in the unoccupied local density of states near the Fermi level, which shift towards E_F with decreasing Fe concentration for both alloys investigated here. The reduction of magnetization with decreasing Fe concentration can be explained by a simple model of *d*-band filling, similar to the explanation of the Slater-Pauling curve for binary alloys. We observe a maximum value for T_C and for the Kerr rotation for the pure Fe/W(110) monolayer, in contrast to the behavior of bulk alloys where maximum values are obtained for Co-Fe alloys.

DOI: 10.1103/PhysRevB.69.134418 PACS number(s): 75.70.Ak, 68.55.Nq, 75.50.Bb, 68.37.Ef

I. INTRODUCTION

The dependence of magnetic and electronic properties of binary alloys on their composition has been studied since a very long time for bulk materials. The most prominent property is the magnetization that varies with the average number N of electrons per atom (Slater-Pauling curve).[1] Ferromagnetism appears for $24 \leqslant N \leqslant 28.6$ with a maximum at $N = 26.3$. An intriguingly simple model for the explanation of magnetic properties of disordered alloys is the rigid band model. In this model it is assumed that the band structure remains independent of the alloy composition while the Fermi level increases with N. The rigid band model is motivated by the electronic structure of $3d$ transition metals being usually discussed in terms of itinerant electrons, i.e., the local atomic properties of disordered alloys may play a less important role compared to the average potentials.

The electronic structure of ferromagnetic transition-metal alloy films is of considerable interest for applications in spintronic devices.[2] The spin polarization of electronic states at the Fermi level controls the performance of tunneling magnetoresistors and spin injection devices.[3] Using ultrathin alloy films deposited at the crucial interfaces one can exploit particular features of their electronic structure near the Fermi level, which in turn can be tuned by the alloy composition. While the electronic structures of bulk alloys are quite well understood,[4,5] ultrathin alloy films are still challenging. It would be fascinating to see that to what extent the magnetic and electronic properties of ultrathin films with a two-dimensional character can be described by similar models as used for bulk materials.

Recently, it was shown that pseudomorphic (ps) $Co_{1-x}Fe_x$ /W(110) monolayers reveal a decreasing Curie temperature with decreasing Fe concentration, in contrast to the behavior of bulk alloys.[6,7] Tentatively, this behavior was described by a rigid band model, considering an increase of the Fermi level with increasing number of electrons.[7] The increasing Fermi level causes a decrease of the density of states at the Fermi energy which in turn would explain the decrease of T_C in the Stoner model. In order to test this hypothesis we conducted the analogous experiment with ps-Fe_xMn_{1-x}/W(110) monolayers. In this case the substitution of Fe with Mn reduces the number of electrons.

Transition-metal alloy films provide the advantage that their structure can be modified by a proper choice of the substrate.[8–10] Structural phase transitions, regularly occurring with varying composition of binary alloys (for Fe-Mn see, i.e., Ref. 11), may be suppressed and the mean nearest-neighbor distance is kept constant. Thus, the pure influence of the alloy composition on the electronic properties can be isolated. The ultrathin limit of transition-metal alloy monolayers on the high melting metal Mo and W forms an ideal prototype for this type of studies, because the larger free-surface enthalpy in comparison to the free-surface enthalpies of the transition metals allows for the preparation of pseudomorphic, thermodynamically stable monolayers. This was shown experimentally for the Fe/W(110) monolayer that served as a model system for a ferromagnetic quasi-two-dimensional system.[12–15] A similar growth mode was found for ps-Mn/W(110) monolayers[16] that show antiferromagnetic order at low temperatures.[17] The growth of ps-Co/W(110) monolayers(ML) is more complicated since a phase transition to a close-packed structure occurs before the monolayer is complete.[18,19] Although theoretically predicted no ferromagnetic order was found experimentally for the ps-Co monolayer.[20]

As was shown previously pseudomorphic and thermodynamically stable $Co_{1-x}Fe_x$ alloy monolayers can be grown on W(110).[6,7] Here we show that Fe_xMn_{1-x} monolayers grow pseudomorphically and are thermodynamically stable on W(110) too, independent of the alloy composition, and that the Curie temperature and the Kerr rotation decrease

with decreasing Fe concentration for the Fe_xMn_{1-x}/W(110) monolayer. This observation is qualitatively similar to previously measured properties of Au/$Co_{1-x}Fe_x$/W(110) (Ref. 7) and $Co_{1-x}Fe_x$/W(110) (Ref. 6) monolayers. Furthermore we will show that the local density-of-states maxima for unoccupied states, as measured by scanning tunneling spectroscopy (STS), shift continuously towards the Fermi level with decreasing Fe concentration. The shift is observed for Fe_xMn_{1-x}/W(110) and $Co_{1-x}Fe_x$/W(110) and is in qualitative agreement with simple models for bulk alloys.

II. EXPERIMENT

The experiments were carried out using an ultrahigh vacuum chamber ($p<1\times10^{-10}$ Torr) equipped with a 4-grid low-energy electron diffraction(LEED) optics and an Omicron ''Micro-STM'' for measurements at room temperature. The single crystal W(110) surface was cleaned by cycles of annealing in an oxygen atmosphere and subsequent flashing at 2000 K. As a consequence of the transferability of the sample, the thermocouple could not be fixed to the sample itself, but only to the sample holder, and absolute temperatures could be obtained only with an error of about ±10 K.

Mn, Fe, and Co (99.99% purity) were deposited simultaneously from BeO crucibles with a rate of 0.1 ML/min and at a substrate temperature of 780 K. The pressure increases during evaporation to $p=2\times10^{-10}$ Torr. The evaporation rate was monitored by a quartz balance which in turn was calibrated by scanning tunneling microscopy (STM) images of pure element coverages $\Theta\leqslant0.5$ where pseudomorphic growth is warranted from previous investigations[16,18,21] for the three elements Fe, Co, and Mn. $\Theta=1$ corresponds to the coverage of one ps monolayer. In addition to samples of homogeneous composition we prepared samples with a linearly varying composition profile (4 mm width) and homogeneous coverage using a two shadowmask technique.

Magnetic properties were investigated in the preparation stage by Kerr magnetometry (wavelength of light 670 nm) as described in Ref. 13. Using a compensation technique, we measured the Kerr rotation in absolute units, as a function of temperature T and external field H. The external field was applied along $[1\bar{1}0]$, i.e., along the easy axis.

STS was performed to obtain differential conductance dI/dU spectra, using a lock-in technique with a 1.65 kHz bias voltage modulation of 50 mV. All bias voltages given are sample voltages with respect to the tip. The data shown here are measured using a $Pt_{80}Ir_{20}$ tip that was cut under tensile stress from a thin wire.

III. MAGNETIC PROPERTIES

Magnetization loops were measured during warming up with a rate of roughly 5 K/min at 100 K decreasing to 1 K/min at 200 K, after cooling with liquid nitrogen to about 100 K. One loop was measured in 120 sec, thus limiting the temperature resolution to 10–2 K in the range from 100 K to 200 K. Figure 1 shows loops for an $Fe_{0.9}Mn_{0.1}$/W(110) submonolayer film with a coverage of $\Theta=0.7$ ML. At the lowest temperature, $T=144$ K, we observe an easy axis loop, where remnance equals the saturation signal. The remagnetization process is spread over a field range of 40 mT with a coercive field $\mu_0H_c=20$ mT. The loop confirms that the easy axis is along $[1\bar{1}0]$, similar to Fe/W(110) and $Co_{1-x}Fe_x$/W(110) submonolayers. Easy axis loops are obtained up to $T=160$ K. For higher temperatures we see a transition to a paramagnetic behavior.

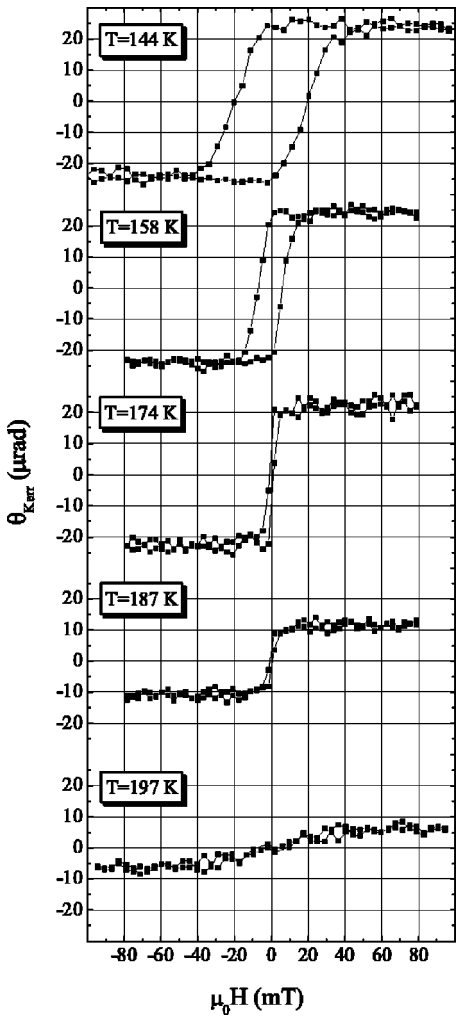

FIG. 1. Magnetization loops measured for an $Fe_{0.9}Mn_{0.1}$/W(110) submonolayer film ($\Theta=0.7$ ML) at the temperatures indicated in the figure. External field was applied along $[1\bar{1}0]$.

Temperature-dependent data for the remnant and saturation Kerr rotation, $\theta_{K,r}$ and $\theta_{K,s}$, were obtained from loops with a reduced number of data points [see Fig. 2(a)]. The remnant signal vanishes at the Curie temperature $T_C=180$ K, while the saturation signal measured at $\mu_0H=0.1$ T can be detected up to $T_s=200$ K. A power-law fit for the remnant value below T_C is not satisfactory because of the fact that $\theta_{K,r}$ is nearly constant below $T=160$ K. The observed temperature dependence of $\theta_{K,r}$ can instead be described by the analytic two-dimensional(2D) Ising function convoluted with a Gaussian distribution of T_C values.[14,22,23] A distribution of T_C values (width $0.1T_C$) can be attributed to the broad distribution of terrace widths (in contrast to the

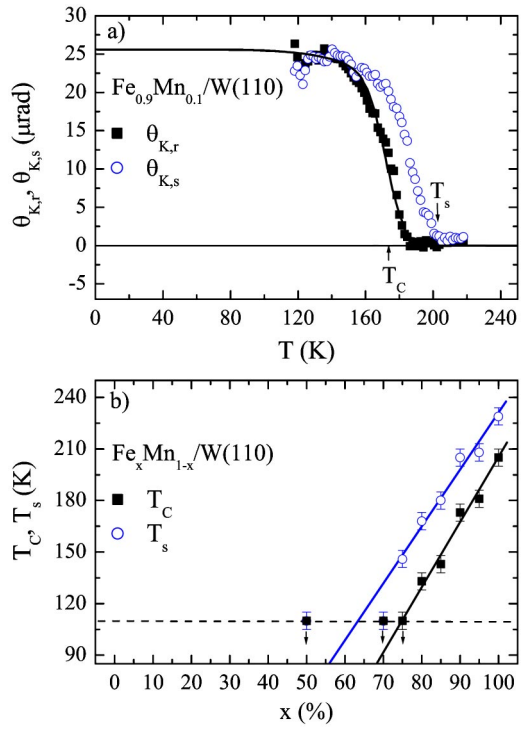

FIG. 2. (a) Dependence of the remnant and saturation Kerr rotation, $\theta_{K,r}$ and $\theta_{K,s}$, on temperature for an $Fe_{0.9}Mn_{0.1}/W(110)$ submonolayer film ($\Theta = 0.7$ ML). The solid line represents a fit of $\theta_{K,r}$ to the two-dimensional Ising function convoluted with a Gaussian distribution of T_C. (b) Dependence of the Curie temperature T_C on the alloy composition of a $Mn_{1-x}Fe_x$ submonolayer ($\Theta = 0.7$). T_C values that are accompanied by a down arrow must lie below the temperature shown.

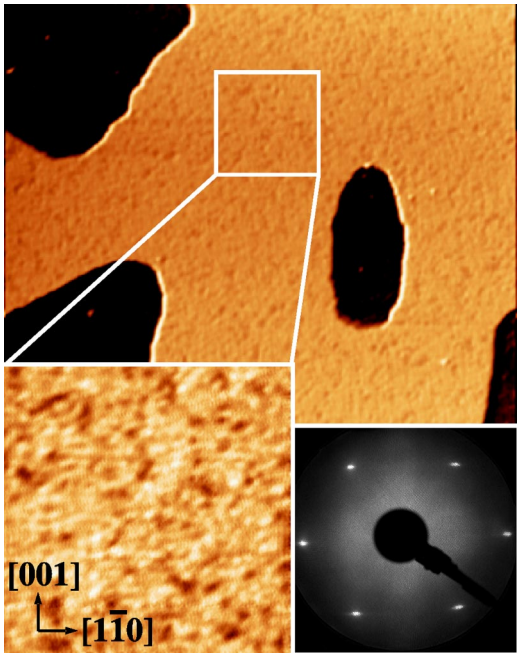

FIG. 3. STM image (115×115 nm^2) of an $Fe_{0.6}Mn_{0.4}/W(110)$ submonolayer film ($\Theta = 0.7$ ML). Tunneling parameters are $I = 500$ pA, and $U = 1$ V. The adsorbed monolayer appears light gray while the uncovered W(110) surface is black. The magnified section (23×23 nm^2) of an area covered by the pseudomorphic submonolayer reveals inhomogeneities with a corrugation of 40 pm, which might be attributed to the random alloy structure. The LEED pattern ($E_i = 80$ eV) shows the bcc(110) structure and confirms the pseudomorphic growth.

substrate used in Ref. 14) of the W(110) substrate surface as observed by STM. We obtained similar data for a series of samples with constant coverage and varying Fe concentration x. The coverage is not an important parameter since for pure Fe/W(110) submonolayers it was shown that T_C depends only weakly on the coverage. The total error for the determination of the concentration x was estimated to $\Delta x = 0.05$. Figure 2(b) summarizes values for T_C and T_s. The Curie temperature T_C decreases almost linearly with increasing Mn content. The critical temperature T_s is about 20 K higher than T_C with a slightly increasing difference with decreasing Fe concentration x. When the Mn content exceeds 25% ($x < 0.75$) no magnetic signal could be detected at the lowest achievable temperature [see Fig. 2(b)]. One should note that the Kerr effect is not sensitive to a possibly present antiferromagnetic order. Assuming the same reduction factor for the Curie temperature and for the Néel temperature when comparing monolayer with bulk alloys, one would expect a Néel temperature of 100 K for the FeMn monolayer, decreasing for higher Fe concentrations.

The observed decrease of T_C with decreasing Fe concentration is in agreement with the properties of bulk Fe-Mn alloys. The Curie temperature of bulk bcc Fe decreases at the rate 15 K/at. % with increasing Mn content.[11] For the monolayer we observed a rate of 4 K/at. %. Because the Curie temperature of the Fe/W(110) monolayer [T_C(Fe) = 225 K] is considerably smaller than the Fe bulk value [T_C(Fe) = 1043 K] it is useful to compare the normalized rates $[dT_C(x)/dx]/T_C(\mathrm{Fe})$. For the monolayer we obtain $[dT_C(x)/dx]/T_C(\mathrm{Fe}) = (1.8 \pm 0.2) \times 10^{-2}$ /at. %, while the corresponding bulk value (1.4×10^{-2} /at. %) is only slightly smaller. Note that the bulk value for Fe-Mn alloys can be determined only for large Fe concentrations $x > 0.97$ because of the occurrence of metastable martensitic phases at larger Mn concentrations and the transition to a stable fcc random alloy phase for $x < 0.7$. These phase transitions are suppressed for $Mn_{1-x}Fe_x/W(110)$ monolayers.

IV. STRUCTURE AND ELECTRONIC PROPERTIES

Figure 3 shows the morphology of an $Fe_{0.6}Mn_{0.4}/W(110)$ submonolayer on a particularly large terrace. There is no substrate step edge visible in the STM image. The adsorbed monolayer forms large compact areas. Because of the large free-surface enthalpy of the W substrate, the monolayer is thermodynamically stable, i.e., islands of more than monolayer thickness do not appear even at higher annealing temperatures. The LEED pattern shows a sharp $p(1 \times 1)$ structure similar to the W bcc(110) surface, thus confirming the pseudomorphic structure of the adsorbed alloy monolayer. The same LEED pattern was observed for all Fe concentrations $0 \leqslant x \leqslant 1$. From the LEED pattern we conclude that Fe and Mn atoms occupy exclusively regular W lattice sites.

Phase separation of adsorbed atoms has to be taken into account even for completely miscible bulk alloys.[24–26] In order to exclude a phase separation for the $Fe_{0.6}Mn_{0.4}$/W(110) monolayer, we measured STM and STS images with high resolution. The magnified section in Fig. 3 reveals a grain structure with a mean grain size of 0.5 nm corresponding to a few unit cells only. The maximum height corrugation amounts to 40 pm. STS images lead to the same result. We attribute the grain structure to a varying distribution of Fe and Mn atoms in the monolayer resulting in a varying electronic structure depending on the number of Fe (or Mn) atoms in the unit cell. The observed compositional fluctuation is close to a random distribution. In contrast to the case of $Co_{1-x}Fe_x$/W(110) we could not find superstructures in the LEED pattern, which would indicate ordered alloy structures.

For the spectroscopic measurement we prepared a series of Fe_xMn_{1-x}/W(110) and $Co_{1-x}Fe_x$/W(110) submonolayer films with varying Fe concentration. Spectroscopic dI/dU curves were recorded on top of the pseudomorphic monolayer areas directly after preparation. The stabilization parameters ($U=+1$ V, $I=0.5$ nA), applied before the feedback loop was opened for measuring the tunneling spectra, were kept constant. These parameters determine the tip distance from the surface and strongly influence the relative peak heights.[17] Spectra were measured with increasing sample bias starting at $U=-1$ V. A comparison of this data to spectra measured with decreasing voltage confirms that peak positions are not significantly shifted. In order to reduce the noise we averaged at least ten single spectra taken at random positions on each structure. This procedure also averages local variations of the electronic structure. Results are summarized in Figs. 4 and 5. We focused on the spectra for positive sample bias, i.e., with electrons tunneling from the tip into unoccupied states of the sample. For positive sample bias the influence of tip states is expected to be less prominent. The tunneling spectra show significant structures continuously varying with composition. For Fe_xMn_{1-x}/W(110), we observe a shoulder at $\Delta E=E-E_F=2.3$ eV for the pure Fe monolayer, which shifts to a lower value $\Delta E=1.8$ eV for the pure Mn/W(110) monolayer with increasing Mn content. For $x=1$ a peak can be seen at $\Delta E=0.3$ eV that rapidly disappears with increasing Mn content but shows up again at a lower energy for $x=0.2$ and $x=0.3$. The spectra for the pure element monolayers are similar to the spectra shown in Refs. 17 and 27.

dI/dU curves for $Co_{1-x}Fe_x$/W(110) monolayers are presented in Fig. 5. For monolayers with $x<0.5$ we took care that spectra were measured on pseudomorphic areas only, since part of the surface transforms into a close-packed structure (see Ref. 7) for higher Co concentrations. The shoulder at $\Delta E=2.3$ eV for $x=1$ disappears immediately for $x<1$ but reappears again for $x<0.5$. The weak peak observed for pure Fe near the Fermi energy at $\Delta E=0.3$ eV develops into a prominent peak for the pure Co monolayer.

For both sets of dI/dU spectra we observe a discontinuous variation of the background, particularly at larger sample bias voltages. The exponentially increasing differential conductivity can be explained by the tunneling transmission probability T:[28]

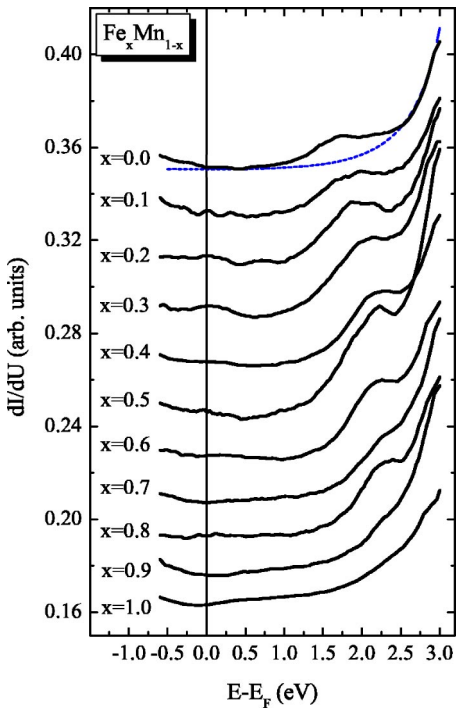

FIG. 4. Differential conductivity (dI/dU) spectra measured on ps-monolayer areas of Fe_xMn_{1-x}/W(110). Data shown result from an average of approximately ten individual spectra. The sample voltage modulation is 50 mV and the tip was stabilized at $U=1$ V and $I=0.5$ nA. The dotted line indicates the tunneling transmission function [see Eq. (2)].

$$T(S,\xi)=\exp\left[-2S\left(\frac{2m}{\hbar^2}(\bar{\Phi}-\xi)\right)^{1/2}\right], \tag{1}$$

with $\xi=(E-eU/2)$. S is the tip surface separation and $\bar{\Phi}$ denotes the effective work function. This function depends sensitively on the local surface potential and the effective area of tip-surface contact that can vary after each tip approach. In order to compare the spectra of different samples we normalize the dI/dU spectra by the symmetric tunneling transmission function

$$F(S,U)=A[T(S,eU/2)+T(S,-eU/2)], \tag{2}$$

where A is the proportionality coefficient related to the tip-surface effective contact area and proportional to the tip and the sample densities of states at the Fermi level, respectively. Theoretically, it was shown that this normalization leads to the best sample density-of-states (DOS) recovery.[28] Recent experiments on Mn(001) surfaces confirm the application of this normalization.[29] The parameters A, S, and Φ are determined by a fit to the dI/dU spectra at the lowest values and at the high-energy cutoff at 3 eV.

Figure 6 shows normalized spectra $(dI/dU)/F$ for the pure Fe/W(110) monolayer and for alloy compositions at the boundary of the ferromagnetic region. The weak peaks and shoulders observed in the original dI/dU spectra appear

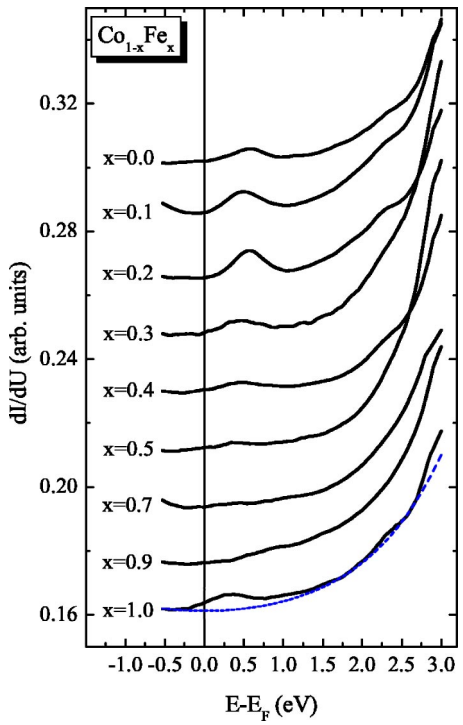

FIG. 5. Differential conductivity (dI/dU) spectra measured on ps-monolayer areas of $Co_{1-x}Fe_x$/W(110). Data shown result from an average of approximately ten individual spectra. The sample voltage modulation is 50 mV and the tip was stabilized at $U=1$ V and $I=0.5$ nA. The dotted line indicates the tunneling transmission function [see Eq. (2)].

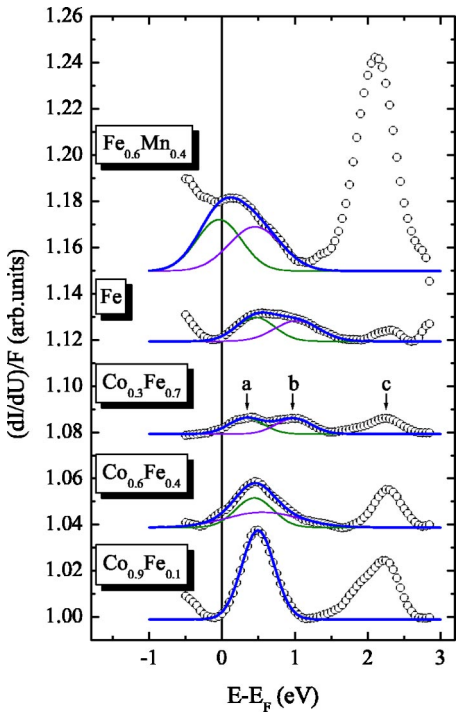

FIG. 6. Differential conductivity (dI/dU) spectra (open circles) normalized to the voltage-dependent tunneling transmission function F, which were obtained for pseudomorphic $Co_{1-x}Fe_x$/W(110) and Fe_xMn_{1-x}/W(110) monolayers. The $(dI/dU)/F$ curves were fitted by two Gaussian peak functions (solid lines).

much more pronounced in the normalized spectra. Spectra for different compositions can be clearly distinguished. It is not possible to fit the spectra observed for binary compounds by a weighted average of the spectra observed for pure element monolayers. This observation indicates that the electronic structure at the Fermi level of the alloy monolayers is a unique property of the binary alloy monolayer rather than the sum of local properties of adsorbed atoms. For the pure Fe/W(110) monolayer the normalized spectrum $(dI/dU)/F$ shows a prominent feature with a maximum at $U=+0.5$ V (see also Ref. 27). This feature may be attributed to unoccupied surface states that have been calculated both for Fe/W(110) (Ref. 30) and Fe/Mo(110) (Ref. 31) revealing a prominent double-peak structure in the local (LDOS) function at slightly higher energies ($0.8\ \text{eV}<\Delta E<1.4\ \text{eV}$).[30] We tentatively fitted this feature by two Gaussian peak functions a and b with maxima at $E_a=+0.5$ eV and $E_b=+1.1$ eV. This fit was applied to all the spectra obtained for the binary alloy monolayers. For all samples, the set of two peak functions fits the $(dI/dU)/F$ curve for unoccupied states surprisingly well. The energy positions of the peaks resulting from the fits are shown in Fig. 7. In addition to the peaks a and b near E_F we observe a narrow intensity maximum (c) near $E_c=+2$ eV.

The experimental results of $(dI/dU)/F$ obtained from all samples of pseudomorphic monolayers of $Co_{1-x}Fe_x$/W(110) and Fe_xMn_{1-x}/W(110) are summarized as an intensity map in Fig. 7. The intensity map represents to a first approximation directly the LDOS above the sample surface for unoccupied states. The x axis represents the total number of electrons per atom varying from Mn ($N=25$) on the left to Co ($N=27$) on the right. The most prominent intensity appears for the equiatomic $Fe_0.5Mn_{0.5}$/W(110) monolayer at an energy of $+2.1$ eV belonging to the feature c. The maximum intensity shifts linearly from $E_c=1.7$ eV for Mn/W(110) $N=25$ ($x=0$) to $E_c=2.1$ eV for $N=25.4$ ($x=0.4$) and further to $E_c=2.3$ eV for $N=26$ ($x=1$) [Fe/W(110)], revealing a kink at $N=25.4$ ($x=0.4$). Feature c becomes rather weak for high Fe concentrations for both alloys but gains again intensity for $Co_{1-x}Fe_x$/W(110) with $x<0.5$, i.e., for $N>26.5$. The energy $E_c=2.3$ eV does not depend on x for $Co_{1-x}Fe_x$/W(110).

Spectral features a and b are comparatively weaker and appear at the highest energy for the pure Fe/W(110) monolayer, shifting to lower-energy values for decreasing Fe concentration. For $Co_{1-x}Fe_x$/W(110) the two peaks a and b collapse into one intense peak at $x=0.2$, i.e., for $N=26.8$.

V. DISCUSSION

For the discussion of the spectral features observed in Fig. 7 we compare the tunneling spectra observed for the pure element monolayers with theoretical calculations. For Mn/W(110) a band-structure calculation has been performed considering particularly tunneling spectroscopy.[17] Peaks in the differential conductivity that were predicted theoretically and consistent with the experiment are located at $E-E_F$

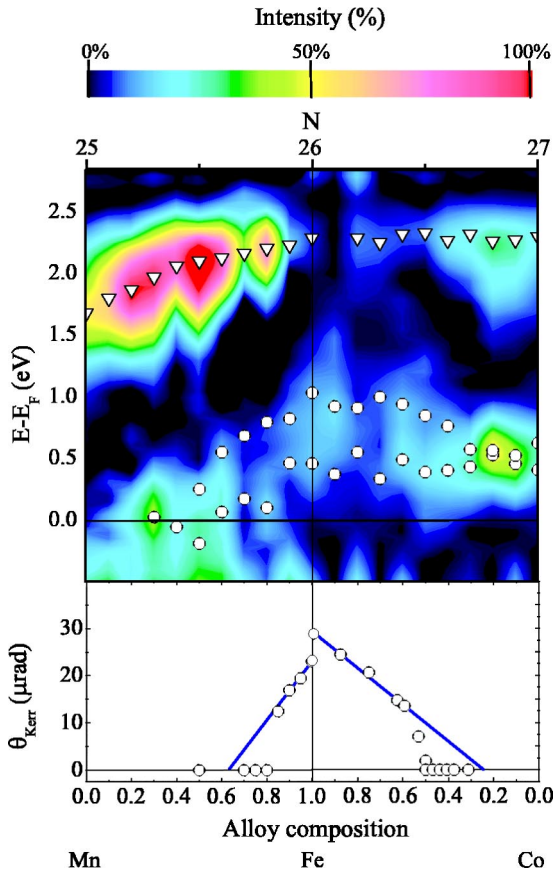

FIG. 7. Intensity map of the normalized differential conductivity spectra $(dI/dU)/F$ for pseudomorphic monolayers of $Co_{1-x}Fe_x$/W(110) and Fe_xMn_{1-x}/W(110). Maxima of the Gaussian peak functions for the features *a* and *b* are indicated by open circles. Open triangles indicate the maxima of peak *c*. The lower panel shows the Kerr rotation θ_K measured at a constant relative temperature $T/T_C=0.9$ for Fe_xMn_{1-x}/W(110). Similar data for Au covered $Co_{1-x}Fe_x$/W(110) monolayers are taken from Ref. 7.

$=-0.4$ eV and $+1.7$ eV,[17] similar to our observation. The peak at $E-E_F=-0.4$ eV was assigned to an occupied surface state while the peak at $+1.7$ eV is identified with a laterally constant part of the calculated DOS, i.e., flat "*d* states." For the Fe/W(110) monolayer a prominent double-peak structure in the calculated LDOS function at 0.8 eV $<\Delta E<1.4$ eV (Ref. 30) was attributed to unoccupied minority surface states. This feature may be related to the peaks *a* and *b* observed in the $(dI/dU)/F$ curve (see Fig. 6). A flat *d*-band structure calculated at $+2.2$ eV (Ref. 30) both for minority and majority electrons might be responsible for the feature *c*. For Co/W(110) a flat *d*-band complex for majority and minority states at the $\bar{\Gamma}$ point was calculated at $+2.5$ eV (Ref. 32) that might be identified with the corresponding peak observed in our case. Note that the Co/W(110) monolayer is ferromagnetic in theoretical calculations (at $T=0$ K) (Ref. 32) while ferromagnetism was not found in experiments at finite temperatures. For the alloy spectra it is a reasonable assumption that the observed intensity maxima (LDOS maxima) are caused by similar features in the band structure as for the pure elements.

The most simple model for disordered binary alloy systems is the rigid band model, i.e., the band structure is independent of the alloy composition while the Fermi level shifts with the average number of electrons per atom. This model is obviously too simple for our alloy monolayers, because it does not explain the experimental result (see Fig. 7). However, for $Co_{1-x}Fe_x$ monolayers one would expect a shift of the bands towards the Fermi energy with increasing Co concentration. This is indeed observed at least for the LDOS feature close to the Fermi level. For Fe_xMn_{1-x} monolayers a shift of the bands to higher energies is expected at first glance since the Mn atom has one *d* electron less compared to Fe. But as already considered by Friedel[33] for bulk alloys, the energy states of manganese may be strongly perturbed, because of their negative nuclear charge $(\Delta Z=-1)$ with respect to Fe, to such an extent that they pass up through the Fermi level and so empty their electrons into the unoccupied minority $3d$ states. By this transfer the *d*-state derived features in the LDOS shift towards E_F.

In order to compare the LDOS features in Fig. 7 with the magnetic properties, we plotted the Kerr rotation as a function of alloy composition on the same *x* axis. In this work we measured the Kerr rotation θ_K for uncovered Fe_xMn_{1-x}/W(110) monolayers at a constant relative temperature $T/T_C=0.9$ representing a value roughly proportional to the ground-state value. For Au covered $Co_{1-x}Fe_x$/W(110) monolayers we present previously published data, Ref. 7. A comparison of data for uncovered and Au covered monolayers is justified here because nearly identical results were shown for the uncovered $Co_{1-x}Fe_x$/W(110) system,[6] although one should note that a coverage may change the electronic properties.

From the study of the thickness dependence of the Kerr rotation for $Co_{1-x}Fe_x$/W(110) layers[7] one obtains the information that the specific Kerr rotation varies only little with *x*, in rough agreement with the compositional dependence of the magnetization for bulk alloys. Details are different, i.e., the maximum of the Kerr rotation occurs for $x=0.5$ while the maximum moment is found for $x=0.7$. The numerical variation of magnetization and Kerr rotation is of the order of 10%. Therefore, it might be assumed that for alloy monolayers the Kerr rotation is a rough measure for the magnetization.[7]

The decrease of magnetization at low temperatures observed for Au/$Co_{1-x}Fe_x$/W(110) monolayers with increasing *N* might be attributed to a filling of *d* holes, similar to the properties of alloys on the right branch of the Slater-Pauling curve. The rapid vanishing of the magnetic signal near $N=26.5$ is certainly due to the finite temperature in combination with the reduction of T_C. This simple assumption of *d*-hole filling does not quantitatively explain the reduction: The initial reduction of the Kerr rotation with increasing *N* corresponds to a reduction of $\Delta\mu=-2.9\mu_B$ per additional *d* electron.[7] This is in sharp contrast to the Slater-Pauling behavior of $\Delta\mu=-1\mu_B$ per electron. For Fe_xMn_{1-x} alloys Friedel's model[33] would predict a reduction of $\Delta\mu/\Delta x=-(\Delta Z+10)\mu_B=-9\mu_B$/atom. For Fe_xMn_{1-x} monolayers we obtain a value of $\Delta\mu/\Delta x=-(8\pm2)\mu_B$/atom.

For both compounds T_C decreases with decreasing Fe

concentration. In the case of $Au/Co_{1-x}Fe_x/W(110)$ monolayers this decrease was explained by the Stoner model that relates T_C to the total DOS at the Fermi level $N(E_F)$ in the paramagnetic state.[7] For bulk Fe, theoretical results showed that the Fermi level is below the maximum of the paramagnetic DOS.[4] The spin-resolved DOS of bulk Fe shows sharp maxima at E_{up} below the Fermi energy for majority electrons and at E_{down} above the Fermi energy for minority electrons. The energy difference $E_F - E_{up}$ is smaller than $E_{down} - E_F$. Consequently, the mean value $E_{down} + E_{up}/2$ is above E_F as expected from the paramagnetic result. A similar evaluation of the spin-resolved DOS for the Fe/W(110) monolayer[30] leads to $(E_{down} + E_{up})/2 < E_F$. Therefore, we estimate that the maximum of the paramagnetic DOS is below E_F. Consequently, the increasing band filling leads to a decrease of $N(E_F)$ and as a consequence of the Stoner model reduces T_C. The shift of electron states towards E_F with increasing Co concentration, which was tentatively assumed in Ref. 7, is now directly observed in the tunneling spectra. The decrease of T_C observed for Fe_xMn_{1-x} monolayers can be explained by the same argument taking into account that the partial replacement of Fe atoms by Mn atoms shifts the electron states near the Fermi level towards E_F similar to the partial replacement of Fe atoms by Co atoms.

VI. SUMMARY

In summary, we have grown pseudomorphic binary alloy monolayers Fe_xMn_{1-x} and $Co_{1-x}Fe_x$ on W(110), where Fe atoms are randomly replaced by Mn or Co atoms. We observe a reduction of the Kerr rotation and a reduction of T_C for $Fe_xMn_{1-x}/W(110)$ monolayers with decreasing Fe concentration. This behavior is similar to previous results obtained for $Au/Co_{1-x}Fe_x/W(110)$ monolayers.[7] STS reveals characteristic maxima in the unoccupied LDOS near the Fermi level, which shift towards E_F with decreasing Fe concentration for both alloys investigated here. The STS study shows that the observed LDOS is an alloy property and not the weighted sum of the LDOS of individual elements. The observed shift of electronic states explains the decrease of T_C by the Stoner model in combination with a recent band-structure calculation for Fe/W(110) monolayers. The reduction of magnetization with decreasing Fe concentration can be explained by a simple model of *d*-band filling, similar to the explanation of the Slater-Pauling curve for binary alloys. Quantitatively, the properties of the alloy monolayers are different from bulk alloys.

(i) We observe a maximum value for T_C and for the magnetization for the pure Fe/W(110) monolayer, in contrast to the behavior of bulk alloys where maximum values are obtained for $Co_{0.3}Fe_{0.7}$ alloys. Whether this difference originates from the 2D character is an open question. In our case only one parameter is varied, namely, the composition, whereas in bulk alloys, the lattice parameter varies with composition.

(ii) On the right side of the Slater-Pauling curve the decrease of the magnetization is significantly faster ($-2.9\ \mu_B$/electron) than the $-1\ \mu_B$/electron (hole filling) value on the bulk curve. This difference cannot be explained by purely optical effects on the Kerr rotation as the electronic structure changes.

ACKNOWLEDGMENTS

We gratefully acknowledge financial support from the Deutsche Forschungsgemeinschaft. We thank U. Gradmann for a critical reading of the manuscript.

[1] S. Chikazumi, *Physics of Ferromagnetism* (Clarendon Press, Oxford, 1997).
[2] G.A. Prinz, Science **282**, 1660 (1998).
[3] P. LeClair, J.T. Kohlhepp, C.H. van de Vin, H. Wieldraaijer, H.J.M. Swagten, W.J.M. de Jonge, A.H. Davis, J.M. MacLaren, J.S. Moodera, and R. Jansen, Phys. Rev. Lett. **88**, 107201 (2002).
[4] P. James, O. Eriksson, B. Johansson, and I.A. Abrikosov, Phys. Rev. B **59**, 419 (1999).
[5] P.H. Dederichs, R. Zeller, H. Akai, and H. Ebert, J. Magn. Magn. Mater. **100**, 241 (1991).
[6] J.P. Pierce, E.W. Plummer, and J. Shen, Appl. Phys. Lett. **81**, 1890 (2002).
[7] M. Pratzer and H.J. Elmers, Phys. Rev. Lett. **90**, 077201 (2003).
[8] F.O. Schumann, R.F. Willis, K.G. Goodman, and J.G. Tobin, Phys. Rev. Lett. **79**, 5166 (1997).
[9] A. Dittschar, W. Kuch, M. Zharnikov, and C.M. Schneider, J. Magn. Magn. Mater. **212**, 307 (2000).
[10] F. Matthes, M. Seider, and C.M. Schneider, J. Appl. Phys. **91**, 8144 (2002).
[11] T. Nishizawa and K. Ishida, *Binary Alloy Phase Diagrams* (ASM, Materials Park, OH, 1986).
[12] U. Gradmann, in *Handbook of Ferromagnetic Materials*, edited by K.H.J. Buschow (Elsevier, Amsterdam, 1993), Vol. 7, p. 11.
[13] H.J. Elmers, Int. J. Mod. Phys. B **9**, 3115 (1995).
[14] H.J. Elmers, J. Hauschild, and U. Gradmann, Phys. Rev. B **54**, 15 224 (1996).
[15] M. Pratzer, H.J. Elmers, M. Bode, O. Pietzsch, A. Kubetzka, and R. Wiesendanger, Phys. Rev. Lett. **87**, 127201 (2001).
[16] M. Bode, M. Hennefarth, D. Haude, M. Getzlaff, and R. Wiesendanger, Surf. Sci. **432**, 8 (1999).
[17] M. Bode, S. Heinze, A. Kubetzka, O. Pietzsch, M. Hennefarth, M. Getzlaff, R. Wiesendanger, X. Nie, G. Bihlmayer, and S. Blügel, Phys. Rev. B **66**, 014425 (2002).
[18] H. Knoppe and E. Bauer, Phys. Rev. B **48**, 1794 (1993).
[19] M. Pratzer, H.J. Elmers, and M. Getzlaff, Phys. Rev. B **67**, 153405 (2003).
[20] G. Garreau, M. Farle, E. Beaurepaire, and K. Baberschke, Phys. Rev. B **55**, 330 (1997).
[21] M. Przybylski, I. Kaufmann, and U. Gradmann, Phys. Rev. B **40**, 8631 (1989).
[22] R.J. Birgeneau, J. Als-Nielsen, and G. Shirane, Phys. Rev. B **16**, 280 (1977).
[23] U. Stetter, M. Farle, K. Baberschke, and W.G. Clark, Phys. Rev. B **45**, 503 (1992).

[24] G. Abadias, A. Marty, and B. Gilles, Acta Mater. **46**, 6403 (1998).
[25] S.-J. Kahng, Y.J. Choi, J.-Y. Park, and Y. Kuk, Appl. Phys. Lett. **74**, 1087 (1998).
[26] S. Krimmel, W. Donner, B. Nickel, H. Dosch, C. Sutter, and G. Grubel, Phys. Rev. Lett. **78**, 3880 (1997).
[27] O. Pietzsch, A. Kubetzka, M. Bode, and R. Wiesendanger, Phys. Rev. Lett. **84**, 5212 (2000).
[28] V.A. Ukraintsev, Phys. Rev. B **53**, 11 176 (1996).
[29] T.K. Yamada, M.M.J. Bischoff, G.M.M. Heijnen, T. Mizoguchi, and H. van Kempen, Phys. Rev. Lett. **90**, 056803 (2003).
[30] X. Qian and W. Hübner, Phys. Rev. B **60**, 16 192 (1999); **67**, 184414 (2003).
[31] T.-H. Rho, Gi-B. Cha, Y. Kwon, C. Lee, and S.-C. Hong, J. Korean Phys. Soc. **35**, 564 (1999).
[32] B. Weimert, J. Noffke, and L. Fritsche, Surf. Sci. **289**, 397 (1993); B. Weimert, Ph.D. thesis, Technical University of Clausthal, Germany, 1995.
[33] J. Friedel, J. Phys. Radium **23**, 501 (1962).